Structural, curvature and electronic properties of Rh adsorption on armchair single-walled carbon nanotube*

Yang Pei-Fang(杨培芳)[a], Wu Feng-Min(吴锋民)[a]†, Teng Bo-Tao(滕波涛)[b], Liu Sha(刘 莎)[a], and Jiang Jian-Zhong(蒋健中)[c]‡

[a] *Institute of Condensed Matter Physics, Zhejiang Normal University, Jinhua* 321004, *China*
[b] *College of Chemistry and Life Science, Zhejiang Normal University, Jinhua* 321004, *China*
[c] *International Center for New-Structured Materials (ICNSM), Zhejiang University and Laboratory of New-Structured Materials, Department of Materials Science and Engineering, College of Materials Science and Chemical Engineering, Zhejiang University, Hangzhou* 310027, *China*

(Received 22 January 2010; revised manuscript received 25 March 2010)

This paper systematically studies the rolling effects of the (n, n) single-wall carbon nanotubes (SWCNT) with different curvatures on Rh adsorption behaviours by using density functional theory. The outside charge densities of SWCNTs are found to be higher than those inside, and the differences decrease with the increase of the tube radius. This electronic property led to the discovery that the outside adsorption energies are higher than the inside ones, and that the differences are reduced with the increase of the tube radius. Partial density of states and charge density difference indicate that these strong interactions induce electron transfer between Rh atoms and SWCNTs.

Keywords: density functional theory, single-walled carbon nanotube, rhodium atom, adsorption
PACC: 7115J, 7125W, 7120C, 7125

1. Introduction

Metallic nanostructures formed by metal atoms adsorbed onto single-walled carbon nanotubes (SWCNTs)[1] can function as electromagnetic devices and catalytic materials.[2−5] The metal atoms adsorbed on the inside of SWCNTs may exhibit different physical and chemical properties than those adsorbed on the outside.[6−9] For example, Pan *et al.*[10] recently reported that the catalytic activity for the conversion of CO and H_2 to ethanol is much higher for Rh particles confined inside carbon nanotubes than for those on the outside of the nanotubes. Our previous work indicated that the adsorption behaviours and electronic structures of Rh inside and outside of the (6, 6) SWCNT are significantly different.[11] In addition, the curvature of the nanotube also affects the physical and chemical properties of adsorbed metal atoms.[12−16] Therefore, two interesting questions are raised regarding how the curvature influences the Rh adsorption behaviours, and how the electronic nature changes for different SWCNTs. In this work, we provide a systematic report on the adsorption behaviours of Rh on armchair SWCNTs with different curvatures and explore their corresponding electronic properties.

2. Models and methods

All of the calculations were performed on the basis of planewave periodic first-principles density functional theory, using the Vienna *ab initio* simulation package (VASP) code.[17,18] The electron exchange and correlation were treated within the generalised gradient approximation (GGA) in the form proposed by Perdew–Burke–Ernzerhof (PBE).[19] The Kohn–Sham one-electron wave functions were expanded in a plane wave basis with cutoff energy at 400 eV; and the electron–core interactions were simplified using the projector augmented wave (PAW) method.[20] A Methfessei–Paxton smearing of 0.1 eV was utilised. Brillouin zone integration was approximated by a summation over special k points using the Monkhorst–Pack scheme. The irreducible Brillouin zone of the SWCNT supercell was sampled with 1×1×6 k-point. The Kohn–Sham equations were solved self-consistently, and the convergence criteria for the energy calculation and structure optimisation

*Project supported by the National Basic Research Programs of China (Grant No. 2006CB708612).
†Corresponding author. E-mail: wfm@zjnu.cn
‡E-mail: jiangjz@zju.edu.cn
© 2010 Chinese Physical Society and IOP Publishing Ltd

were set to: (a) a self consistent field (SCF) tolerance of 1.0×10^{-4} eV and (b) a maximum Hellmann–Feynman force tolerance of 0.01 eV/Å, respectively.

Several (n, n) armchair SWCNTs ($n = 4$, 5, 6, 7, 8, 10) were used as model systems in this work. We used periodic boundary conditions on supercell geometries with sufficient lateral separations between neighbouring tubes (10 Å, 1 Å=0.1 nm). To minimise the adsorbate interactions, we compared the adsorption energies of the supercells with $c_{\rm sc} = 2 - 4c$, where c is the lattice constant of SWCNT along its Z axis. Their differences are less than 0.1 eV. For precision and efficiency, the supercell with $c_{\rm sc} = 2c$ was used in this work. Five possible adsorption sites including the top site, two hollow sites and two bridge sites are shown in Fig. 1. For inside and outside of the SWCNTs, ten initial structures (I–T, I–H1, I–H2, I–B1, I–B2, O–T, O–H1, O–H2, O–B1, and O–B2) were studied in the present work. The letter I and O point to the adatom at the inside and outside of the SWCNT, respectively.

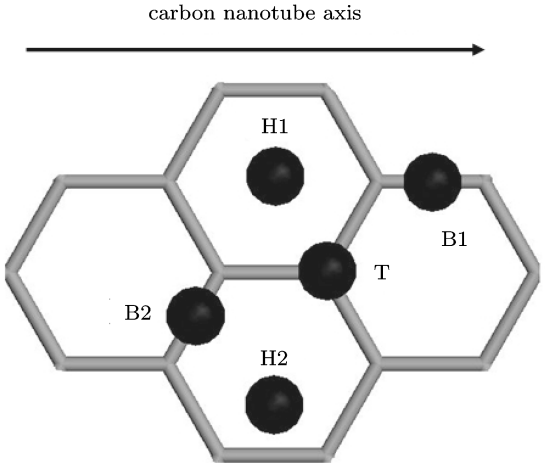


Fig. 1. Adsorption sites for a single Rh atom on an SWCNT.

The adsorption energy of Rh on SWCNT was defined as: $E_{\rm ads} = E_{\rm (Rh/tube)} - E_{\rm tube} - E_{\rm Rh}$, where $E_{\rm (Rh/tube)}$ is the total energy of the tube with the adsorbed Rh atom, and $E_{\rm (tube)}$ and $E_{\rm (Rh)}$ are energies of the SWCNT and an isolated Rh atom, respectively. Therefore, a negative $E_{\rm ads}$ value indicates exothermic adsorption, while a positive one indicates endothermic adsorption. The more negative the energy is the stronger the adsorption is.

3. Results and discussion

All possible initial structures of a single Rh atom adsorbed on the inside or outside of an SWCNT were optimised. The configurations at T and B2 sites were found to be unstable, while others were stable. The optimised sites of adatoms inside and outside the SWCNT are shown in Fig. 2, and the corresponding adsorption energies and the C–Rh bond distances are listed in Table 1. For the I–H1 configurations, the Rh atom locates almost in the centre of the hexagonal ring, seen in Fig. 2(a). As the tube diameter increases, the bond distances of Rh–C_1 and Rh–C_4 increase from 2.14 Å to approximately 2.23 Å. The differences between Rh–C bond distances (C_1 and C_4) and those of (C_2, C_3, C_5, and C_6) decline with increases in tube radius. Due to the rolling effects, the opposite results were observed for the O-H1 configurations. The Rh–C distances (C_1 and C_4) are greater than those of (C_2, C_3, C_5, and C_6). With an increase in radius, the former are shortened, while the latter are lengthened, resulting in a reduction in the differences of Rh–C bonds of O–H1 configurations.

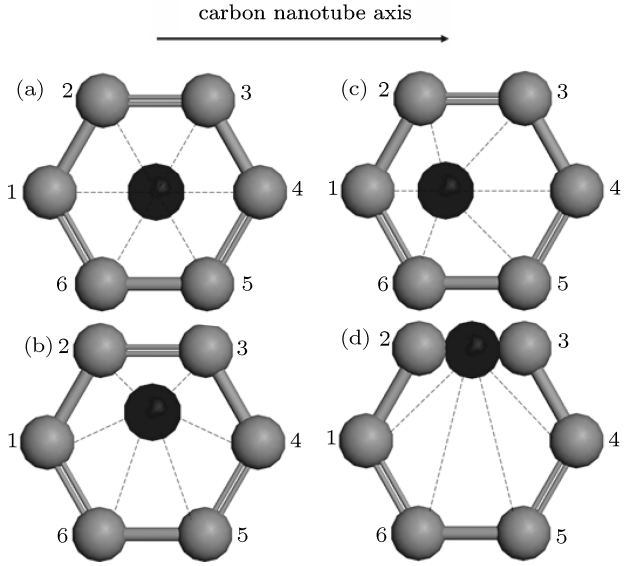


Fig. 2. Optimised sites for a Rh atom on an SWCNT: (a) I–H1 and O–H1; (b) I–H2; (c) O–H2; (d) I–B1 and O–B1.

As shown in Table 1, only I–H2 configurations of the (4, 4) SWCNT were obtained. This might be due to its high curvature, which leads to strong interactions among Rh, C_1, and C_4 atoms. Therefore, the Rh atom on the I–H1 site is unstable and transfers to the I–H2 site. With the increase in the SWCNT radius, the adsorption energies of SWCNTs ($n = 5 - 7$) are almost equivalent. When the tube radius was further increased, only the I–H1 stable configurations were obtained. As shown in Table 1 and Fig. 2(c), the O–H2 configuration is the most stable structure. The adatom deviates from the centre of the carbon ring to

form three Rh–C bonds (C_1, C_2, and C_6). The Rh–C (C_1, C_2, and C_6) bond lengths increase with increasing radius; while the distance of Rh–C bonds (C_3–C_5) shows the opposite trend. For the O–B1 structure, the adatom locates in the middle of the two neighbouring carbon atoms to two Rh–C bonds, seen in Fig. 2(d). As the radius increases, the corresponding bond lengths are elongated.

Table 1. The adsorption energies and the C–Rh bond lengths of stable configurations of (n, n) SWCNT Rh atom.

SWCNT	site	E_{ads}/eV	d_{C-Rh}/Å					
			C_1	C_2	C_3	C_4	C_5	C_6
(4, 4)	I–H2	–1.64	2.147	2.208	2.209	2.147	2.621	2.618
	O–H1	–2.4	2.51	2.222	2.247	2.547	2.244	2.22
	O– H2	–2.7	2.02	2.149	3.072	3.517	3.074	2.15
	O–B1	–2.33	2.958	2.061	2.061	2.958	3.233	3.233
(5, 5)	I–H1	–1.75	2.141	2.339	2.337	2.138	2.357	2.359
	I–H2	–1.76	2.144	2.272	2.272	2.144	2.442	2.443
	O–H1	–2.23	2.492	2.253	2.253	2.492	2.252	2.251
	O–H2	–2.43	2.04	2.171	2.99	3.401	2.99	2.171
	O–B1	–2.13	2.944	2.076	2.077	2.944	3.267	3.266
(6, 6)	I–H1	–1.8	2.148	2.333	2.339	2.161	2.334	2.329
	I–H2	–1.8	2.169	2.232	2.232	2.169	2.477	2.477
	O–H1	–2.14	2.447	2.255	2.275	2.48	2.275	2.255
	O– H2	–2.29	2.055	2.18	2.92	3.304	2.92	2.18
	O–B1	–2.02	2.918	2.086	2.086	2.918	3.272	3.272
(7, 7)	I–H1	–1.85	2.176	2.31	2.31	2.176	2.338	2.339
	I–H2	–1.84	2.177	2.273	2.272	2.177	2.388	2.39
	O–H1	–2.12	2.424	2.262	2.281	2.46	2.272	2.252
	O– H2	–2.23	2.069	2.192	2.883	3.248	2.883	2.192
	O–B1	–1.97	2.944	2.092	2.092	2.944	3.339	3.339
(8, 8)	I–H1	–1.86	2.191	2.343	2.343	2.191	2.296	2.296
	O–H1	–2.08	2.42	2.271	2.274	2.425	2.271	2.268
	O–H2	–2.16	2.065	2.192	2.853	3.201	2.853	2.192
	O–B1	–1.92	2.904	2.096	2.096	2.904	3.3	3.3
(10, 10)	I–H1	–1.9	2.224	2.318	2.318	2.225	2.305	2.305
	O–H1	–2.05	2.396	2.278	2.278	2.394	2.273	2.273
	O–H2	–2.07	2.087	2.203	2.775	3.087	2.774	2.2
	O–B1	–1.86	2.907	2.1	2.1	2.907	3.337	3.337

To further analyse the curvature effects on the adsorption behaviours of the Rh atom inside and outside the (n, n) SWCNT, the adsorption energies versus the tube radius are shown in Fig. 3. Figure 4(a) shows that the adsorption energies of the outside configurations decrease with increasing radius, whereas the inside configurations show the opposite trend. Their differences reduce from 1.06 eV for the (4, 4) SWCNT to 0.17 eV for the (10, 10) tube. As shown in Fig. 4(b), the adsorption energy differences between the O–H1 and O–H2 configurations also gradually decrease with the increase of tube radius. These results can be attributed to the rolling effect of SWCNTs, which leads to the outside charge density being higher than the inside. These differences decrease with the increase of tube radius, which finally tends to become uniform, like the graphene sheet. Therefore, the adsorption energies of Rh on the inside and outside of different SWCNT show similar trends. These results are fully consistent with the data reported by Gülseren *et al.*[10] and Krasheninnikov *et al.*,[13] which show that the adsorption energies of H, C and Al on the outside of SWCNT decrease with the increase of the radius. Therefore, the conclusion presented here reveals a simple physical fact, which might be extrapolated to predict the adsorption energy of adatom on the SWCNT.

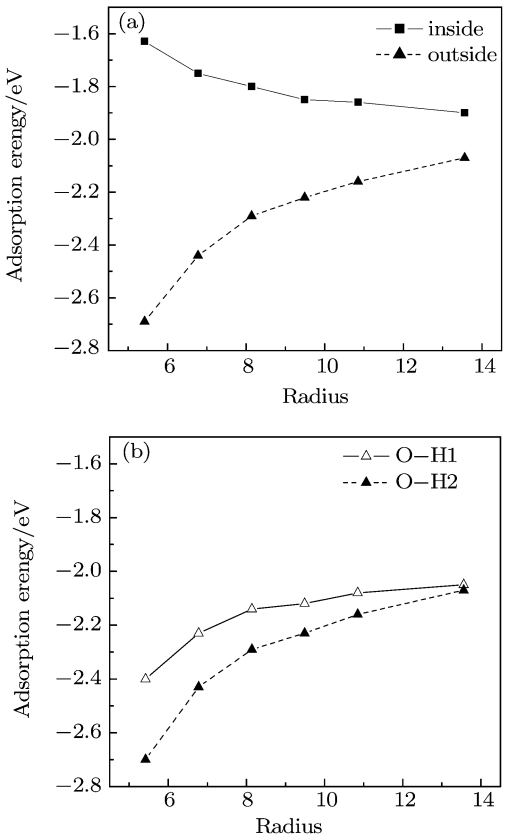


Fig. 3. Adsorption energies for an Rh atom on the (n, n) SWCNTs as a function of tube radius: (a) the most stable inside and outside configurations; (b) O–H1 and O–H2 site.

3.1. Electronic structure

3.1.1. Charge density difference (CDD) of SWCNTs

We further investigated the CDD of typical SWCNTs, (4, 4), (7, 7), and (10, 10), etc. The SWCNT CDD is defined as: $\Delta\rho = \rho_{SWCNT} - n\rho_C$, where ρ_{SWCNT} and ρ_C are the charge densities of an SWCNT and a single carbon atom, respectively. Therefore, the SWCNT CCDs with different curvatures measure the carbon charge redistribution when carbon atoms form

the SWCNTs. The corresponding CDD slices of typical SWCNTs are shown in Fig. 4, in which the red part indicates a gain of electrons, while the blue portion means a loss of electrons. The outside charge density of the (4, 4) tube is clearly much higher than the inside charge. With an increase in radius, the differences are reduced, as seen in Fig. 4(b). Finally, the inside and outside charge densities are almost equivalent when the radius approaches 13.6 Å for the (10, 10) SWCNT. Therefore, as the tube curvature increases, more electrons exist and a stronger corresponding adsorption occurs when Rh adsorbs outside of the SWCNTs. For the inside configurations, the opposite results should be reasonably expected, which are consistent with the above calculations.

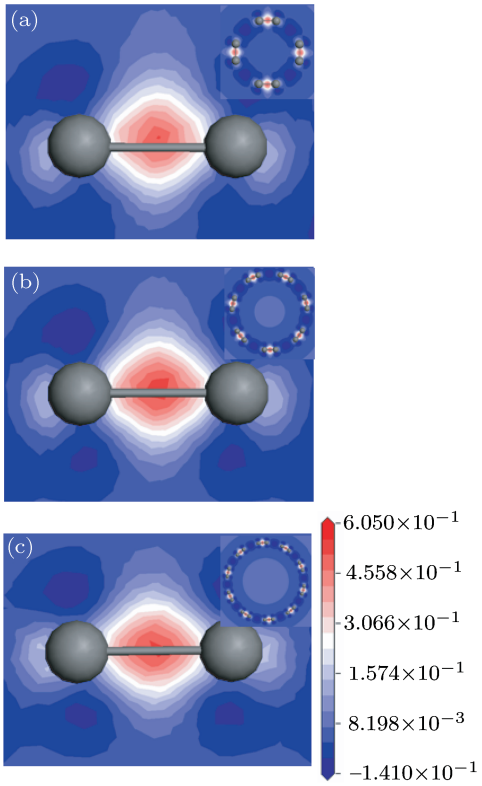


Fig. 4. (Colour on line) Charge density of the bare (n, n) SWCNT: (a) (4, 4); (b) (7, 7); (c) (10, 10).

3.1.2. The partial density of states (PDOS) of Rh inside and outside the SWCNTs

The pronounced curvature effect of SWCNTs leads to a charge redistribution among the carbon atoms, and then results in different adsorption behaviour of Rh. Hence, we investigated the PDOS of Rh inside and outside the typical SWCNTs, as shown in Fig. 5. The valence electrons configuration of an isolated Rh is known to be $4d^8 5s^1$. When Rh adsorbs onto SWCNTs, the PDOS peaks overlap, due to the strong interactions between the adatom and the SWCNTs. According to the crystal field theory (CFT), the electrons redistribute to the 4d orbital, which results in the electrons under the Fermi level being entirely 4d electrons. The PDOS peaks of 5s are all above the Fermi level. For the Rh atom inside of a (4, 4) SWCNT, the PDOS peaks of the spin up and down, are symmetrical in Fig. 5(b), indicating a zero magnetic moment, as listed in Table 2. In contrast, the symmetry of the outside PDOS peaks of the adatom is slightly less the that inside, and its magnetic moment is 0.32 μ_B. With an increase of tube radius, the symmetries of the PDOS peaks decrease and the corresponding magnetic moment gradually increases, seen in Fig. 5(c). When the index n of the SWCNT reaches 10, the inside PDOS becomes quite similar to the outside, and their magnetic moments are almost equivalent, as can be seen in Fig. 5(d). These results

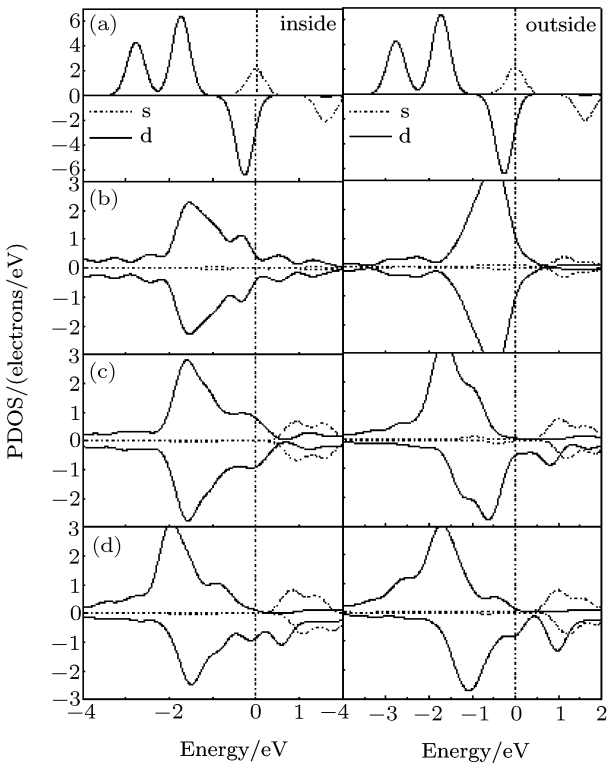


Fig. 5. The PDOS of a single Rh atom adsorbed inside (left) and outside (right) the (n, n) SWCNTs: (a) single Rh; (b) (4, 4); (c) (7, 7); (d) (10, 10). Black line denotes the d electron of Rh, short dash line denotes the s electron, and dashed line denotes the Fermi level.

are in good agreement with the adsorption energies of Rh on SWCNTs. The integral values of the PDOS peaks up to the Fermi level (the occupied electrons of Rh atom) are generally about 7.5–8.5, which is less than that of a single Rh atom, indicating that partial

4d electrons of the Rh atom transfer to the SWCNT upon adsorption. Therefore, the charge of the adatom is positive, while that of the carbon tube is negative. For further validation, the Mulliken charges of the Rh atom are calculated and listed in Table 2. With an increase of tube radius, the Mulliken charge of adsorbed Rh inside SWCNTs decreases. However, the charge of the SWCNT outside increases at first and then remains nearly unchanged until the index n reaches 6.

Table 2. Radius, magnetic moment, and Mulliken charge of the most stable configurations for the adsorbed Rh atom inside and outside the (n, n) SWCNTs.

SWCNT	R/Å	magnetism(μ_B)		mulliken charge	
		inside	outside	inside	outside
(4,4)	5.42	0.00	0.32	1.51	0.52
(5,5)	6.78	0.23	0.56	1.18	0.60
(6,6)	8.14	0.29	0.66	1.05	0.72
(7,7)	9.49	0.35	0.71	0.96	0.67
(8,8)	10.85	0.41	0.75	0.93	0.68
(10,10)	13.56	0.80	0.81	0.94	0.70

3.1.3. The CDD of Rh inside and outside of SWCNTs

To give a further insight into the curvature effects of SWCNTs an Rh adsorption, the CDD of the typical SWCNTs adopting an Rh atom were further studied in Fig. 6. The CDD is defined as: $\Delta\rho = \rho_{\mathrm{Rh/SWCNT}} - \rho_{\mathrm{SWCNT}} - \rho_{\mathrm{Rh}}$, where $\rho_{\mathrm{Rh/SWCNT}}$ is the charge density of the SWCNT with an adopted Rh atom, while ρ_{SWCNT} and ρ_{Rh} are the charge densities of the SWCNT and a single Rh atom, respectively. Therefore, CCDs with different curvatures measure the charge redistribution between the SWCNT and Rh atom upon adsorption. The red part indicates a gain of electrons, while the blue part indicates a loss of electrons. When Rh adsorbs inside the SWCNTs, the electrons lost from an inner Rh atom decrease, while the electrons obtained from SWCNTs increase with the increase of tube radius, indicating that the interactions between Rh and SWCNTs become strong.

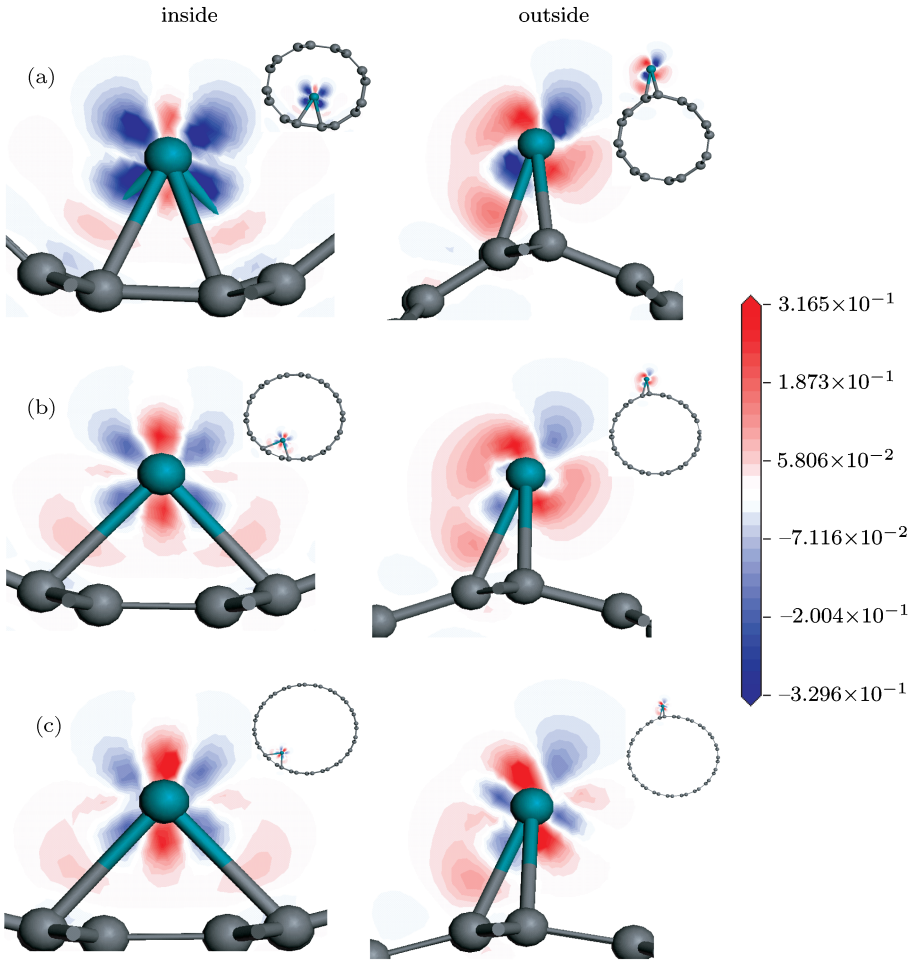


Fig. 6. (Colour on line) The CDD of an Rh atom on the typical SWCNTs, the left is the inside configuration, the right is the outside one: (a) (4, 4); (b) (7, 7); (c) (10, 10).

As a result, the Mulliken charges of Rh decrease, and the adsorption energies increase with the increase of tube radius. Unlike the case for the inner adatom, it can be learned from Fig. 6 that a difference in the charge redistribution for an outside adatom is not obvious with the increase of tube radius. This is consistent with the calculated Mulliken charges of the outside Rh atom, which varies from 0.52–0.70 as the tube radius increases. On the other hand, the electron's overlap of the Rh–C bond shows a slight decrease with the increase of tube radius, which is in agreement with the decrease of adsorption energies. In summary, CDD provides us with an intuitive insight into electron transfer during the adsorption of Rh inside and outside of the SWCNTs with varying tube curvatures.

4. Conclusions

In conclusion, the structures and electronic properties of a single Rh atom inside and outside a series of (n, n) armchair SWCNTs were systematically studied. Due to the rolling effect of SWCNTs, the outside configurations are more stable than the inside ones. With the increase of tube radius, the adsorption energy differences are reduced. The SWCNT CDD reveals the electronic nature of this phenomenon, that is, the outside charge densities of SWCNTs are higher than the inside charge densities, and the differences decrease with the increase of tube radius. The PDOS and CDD analysis indicate that the strong interactions lead to electron transfer between Rh atom and SWCNTs, and explain the Mulliken charge and magnetic moment variation of an Rh atom inside and outside SWCNTs with the increase of tube radius.

Acknowledgments

Calculations of this work were carried out at the Supercomputer of College of Mathematics Physics and Information Engineering of Zhejiang Normal University.

References

[1] Iijima S 1991 *Nature* (London) **354** 56
[2] Yagi Y, Briere T M, Sluiter M H F, Kumar V, Farajian A A and Kawazoe Y 2004 *Phys. Rev.* B **69** 075414
[3] Durgun E, Dag S, Bagci V M K, Gülseren O, Yildirim T and Ciraci S 2003 *Phys. Rev.* B **67** 201401
[4] Ni M Y, Wang X L and Zeng Z 2009 *Chin. Phys.* B **18** 357
[5] Chen G D, Wang L D, An B, Yang M, Cao D C and Liu G Q 2009 *Acta Phys. Sin.* **58** 1190 (in Chinese)
[6] Bagci V M K, Gülseren O, Yildirim T, Gedik Z and Ciraci S 2002 *Phys. Rev.* B **66** 045409
[7] Miao L, Liu H J, Wen Y W, Zhou X and Hu C Z 2008 *J. Appl. Phys.* **103** 016106
[8] Yuan S J, Kong Y, Wen F S and Li F S 2007 *J. Phys.: Condens. Matter* **19** 466203
[9] Yang X B and Ni J 2004 *Phys. Rev.* B **69** 125419
[10] Pan X L, Fan Z L, Chen W, Ding Y J, Luo H Y and Bao X H 2007 *Nature Materials* **6** 507
[11] Yang P F, Hu J M, Teng B T, Wu F M and Jiang S Y 2009 *Acta Phys. Sin.* **58** 3331 (in Chinese)
[12] Gülseren O, Yildirim T and Ciraci S 2001 *Phys. Rev. Lett.* **87** 116802
[13] Krasheninnikov A V, Nordlund K, Lehtinen P O, Foster A S, Ayuela A and Nieminen R M 2004 *Phys. Rev.* B **69** 073402
[14] Gülseren O, Yildirim T and Ciraci S 2002 *Phys. Rev.* B **65** 153405
[15] Zhao M W, Xia Y Y, Ma Y C, Ying M J, Liu X D and Mei L M 2002 *Phys. Rev.* B **66** 155403
[16] Stojkovic D, Lammert P E and Crespi V H 2007 *Phys. Rev. Lett.* **99** 026802
[17] Kresse G and Furthmüller J 1996 *Comput. Mater. Sci.* **6** 15
[18] Kresse G and Furthmüller J 1996 *Phys. Rev.* B **54** 11169
[19] Perdew J P, Chevary J A, Vosko S H, Jackson K A, Pederson M R, Singh D J and Fiolhois C 1992 *Phys. Rev.* B **46** 6671
[20] Blöchl 1994 *Phys. Rev.* B **50** 17953